Academic Journal of Science and Technology
ISSN: 2771-3032 | Vol. 20, No. 1, 2026

Comprehensive Stiffness Modeling and Posture Optimization of Robotic Bonnet Polishing System

Xuezhen Li

School of Mechanical Engineering, University of Shanghai for Science and Technology, Shanghai 200093, China

Abstract: The introduction of a metal rubber vibration damper into a robotic bonnet polishing system can effectively dissipate high-frequency chatter energy and significantly improve the machined surface quality of optical components. However, its inherent porous elastic characteristics inevitably introduce a series compliance link at the end-effector, leading to a decrease in the macroscopic normal static stiffness of the system. This makes it highly susceptible to trajectory deviation and insufficient deformation resistance under polishing contact forces. To seek the optimal balance between "microscopic dynamic vibration reduction" and "macroscopic static high stiffness", this paper investigates comprehensive stiffness modeling and posture optimization methods considering end-effector compliance. First, based on the classical joint stiffness model of industrial robots, the vibration damper is equivalently transformed into a spatial compliance matrix to construct a comprehensive static stiffness analytical model of the polishing system. The anisotropic characteristics of the spatial stiffness at the end-effector are thoroughly analyzed using the compliance ellipsoid theory, and an evaluation index for maximizing normal stiffness oriented to actual processes is proposed. Second, taking redundant posture angles such as the bonnet precession angle as optimization variables, a posture optimization mathematical model based on Particle Swarm Optimization (PSO) is established. This aims to actively compensate for the loss of end-effector stiffness by adjusting the posture of the robot body. Finally, finite element simulations and dwell-spot polishing experiments are carried out. The results demonstrate that the optimization algorithm effectively mobilizes the optimal stiffness direction of the robot body, successfully overcoming the weakness of static deformation while fully leveraging the vibration reduction advantages of the metal rubber. Under the optimized posture, the surface roughness of quartz glass in spot polishing is significantly reduced from 0.101 μm in the conventional posture to 0.025 μm, representing a reduction of 68.3%. This study provides a new perspective for the collaborative control of "vibration reduction and stiffness enhancement" for low-stiffness robots in the field of precision polishing.

Keywords: Bonnet Polishing; Metal Rubber; Comprehensive Stiffness Modeling; Stiffness Balance; Posture Optimization.

1. Introduction

Robotic bonnet polishing technology has been widely applied in high-end manufacturing fields such as aerospace, precision molds, and optical components due to its excellent surface adaptability and stable contact force control capabilities. However, the inherent "weak rigidity" characteristic of serial industrial robots[1] makes their end-effectors prone to elastic deformation and vibration under the continuous action of polishing contact forces, which significantly affects machining stability and the surface quality of polished components.

To address the deformation and vibration issues caused by the weak rigidity of robots, research by domestic and international scholars can generally be classified into two categories: stiffness optimization from the perspective of the robot body, and active or passive suppression research to reduce system vibration. In terms of robot stiffness, Pan et al. [2]investigated a working stiffness evaluation model for robotic bonnet polishing systems and proposed the Normal Stiffness Coefficient (NSC), providing a crucial theoretical basis for further optimizing the working stiffness of robotic machining systems. Qu et al. [3]utilized the self-motion characteristics of redundant robots, identified robot joint stiffness based on a traditional stiffness mapping model, and performed robot posture optimization under the constraints of machining postures and joint angles. Zhu et al. [4]proposed a posture optimization method considering the machining stiffness at the robot end-effector. By combining the spatial directionality of the end-effector stiffness, they established a machining stiffness index, KNF, to optimize the chamfering posture of the robot, which significantly improved machining quality. Regarding robot vibration suppression, Zhou et al. [5]optimized the dynamic characteristics of a robotic bonnet polishing system based on metal rubber vibration reduction technology, demonstrating the significant vibration reduction effect of metal rubber through vibration characteristic analysis and optical component polishing verification experiments. For forging robots, Wang [6] established a flexible manipulator model, designed metal rubber joint dampers, explored the static model and vibration isolation mechanism of metal rubber materials, and determined the optimal metal wire diameter for suppressing the robot's residual vibration through comparative experiments.

It can be observed that research on robot body stiffness primarily focuses on quasi-static stiffness optimization, with insufficient consideration given to suppressing dynamic vibrations during the robotic machining process. When the system lacks sufficient damping, even with high stiffness, machining quality may still degrade due to resonance[7]. Conversely, research on robot vibration reduction emphasizes the damping characteristics and structural design of the device itself, without thoroughly exploring the changes in the overall stiffness of the robot after introducing a flexible vibration damper, thus neglecting the deformation of the robot itself. In summary, existing studies lean toward either stiffness modeling and posture optimization or the design of vibration damping devices, and have yet to integrate both into a unified framework for systematic consideration.

Addressing these research gaps, this paper takes an ABB

IRB2600 robotic bonnet polishing system equipped with a metal rubber vibration damper as the research object. The metal rubber damper is positioned as a key design element within the system that possesses both stiffness and damping attributes, and research is conducted focusing on collaborative stiffness-vibration reduction optimization. First, a comprehensive stiffness model encompassing the robot body and the vibration damper is established to reveal their coupling relationship. Second, combining the compliance ellipsoid theory with the force characteristics of bonnet polishing, an evaluation index for maximizing normal stiffness under the constraint of vibration reduction performance is proposed. Taking the bonnet posture angle as the optimization variable, a multi-constraint posture optimization mathematical model is established, and the Particle Swarm Optimization (PSO) algorithm is employed to solve for the optimal posture. Finally, the accuracy of the comprehensive stiffness model is verified through finite element simulations, and quartz glass polishing experiments are conducted to validate the effectiveness of the optimization method.

2. Comprehensive Stiffness Modeling of the Robotic Bonnet Polishing System

First, the kinematic modeling of the ABB IRB2600 robot is conducted to determine the end-effector pose matrix and the Jacobian matrix. Second, a comprehensive stiffness model incorporating the metal rubber vibration damper is established.

2.1. Robot Kinematics Modeling

The geometric relationships between adjacent links of the robot are described based on the Modified Denavit-Hartenberg (MDH) parameters [8]. These parameters include the link length a_i, link offset d_i, link twist angle α_i, joint angle θ_i, and the joint range, as listed in Table 1.

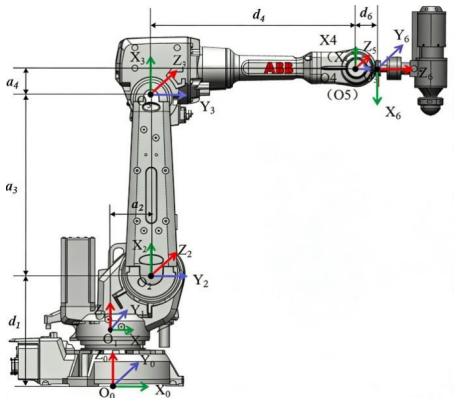

Figure 1. The linkage coordinate system of the ABB-IRB2600 body robot

The homogeneous transformation matrix representing the pose of the robot end-effector relative to the base frame is given by ${}^{0}_{6}T$:

$$ {}^{0}_{6}T = {}^{0}_{1}T\,{}^{1}_{2}T\,{}^{2}_{3}T\,{}^{3}_{4}T\,{}^{4}_{5}T\,{}^{5}_{6}T = \begin{bmatrix} n_x & o_x & a_x & p_x \\ n_y & o_y & a_y & p_y \\ n_z & o_z & a_z & p_z \\ 0 & 0 & 0 & 1 \end{bmatrix} \quad (1) $$

where $\begin{bmatrix} P_x P_y P_z \end{bmatrix}^T$ represents the position vector of frame {6} with respect to frame {0}, and $\begin{bmatrix} n_x n_y n_z \end{bmatrix}^T$, $\begin{bmatrix} o_x o_y o_z \end{bmatrix}^T$, and $\begin{bmatrix} a_x a_y a_z \end{bmatrix}^T$ denote the direction vectors of frame {6} relative to frame {0}.

$$ J(\mathrm{q}) = [J_1 \quad J_2 \quad \cdots \quad J_6] = \begin{bmatrix} z_1 \times {}^{1}p_6^0 & z_2 \times {}^{2}p_6^0 & \cdots & z_6 \times {}^{6}p_6^0 \\ z_1 & z_2 & \cdots & z_6 \end{bmatrix} \quad (2) $$

where z_i is the unit vector along the z-axis of frame {i}, and ${}^{i}p_6^0$ is the position vector of the end-effector's coordinate origin relative to frame {i}, expressed in the base frame {0}.

The derived Jacobian matrix maps the infinitesimal displacements of each joint to the robot's end-effector, establishing a solid foundation for the subsequent static stiffness modeling and analysis of the robot.

2.2. Comprehensive Stiffness Model of the Robot

Based on the derivation of the Jacobian matrix, the classical stiffness model proposed by Salisbury[9] is adopted for analysis. Let the joint stiffness matrix be expressed as:

$$ K_q = diag\left(k_1, k_2, k_3, k_4, k_5, k_6\right) \quad (3) $$

Where k_i represents the equivalent torsional stiffness of the i joint. This model assumes that the link stiffness is significantly higher than the joint stiffness, which is consistent with common simplification approaches in existing research on robot stiffness.

The stiffness matrix in the Cartesian space is given by:

$$ K_{\mathrm{c}} = J^{-T}\left(q\right) \cdot K_q \cdot J^{-1}\left(q\right) \quad (4) $$

By taking the inverse of the joint stiffness matrix, the joint compliance matrix is obtained as:

$$ C_q = K_q^{-1} = \mathrm{diag}\left(\frac{1}{k_1}, \frac{1}{k_2}, \frac{1}{k_3}, \cdots, \frac{1}{k_6}\right) \quad (5) $$

By combining Equations (4) and (5), the Cartesian compliance matrix of the end-effector can be obtained as:

$$ C_c = K_c^{-1} = \left[J^{-T}\left(q\right) \cdot K_q \cdot J^{-1}\left(q\right)\right]^{-1} = J\left(q\right) \cdot C_q \cdot J^{T}\left(q\right) \quad (6) $$

Table 1. Parameter Table of ABB IRB-2600 D-H

Joint i	Joint angle θ_i(°)	Link offsetd_i(mm)	Link twist angleα_i(°)	Link lengtha_i(mm)	Joint range (°)
1	θ1	445	0	0	±180
2	θ2	0	-90	150	-95~155
3	θ3	0	0	700	-180~75
4	θ4	795	-90	115	±400
5	θ5	0	90	0	±120
6	θ6	85	-90	00	±400

From this equation, it can be observed that the calculation of the Cartesian compliance matrix of the end-effector does not require the inversion of the Jacobian matrix. This effectively avoids the singularity issues where the matrix becomes non-invertible when the robot is in a singular posture.

In the bonnet polishing system, a metal rubber vibration damping structure is designed at the connection between the robot's sixth-axis flange and the bonnet polishing device (as shown in Figure 3). This device consists of three layers of metal rubber connected in series, positioned between the sixth-axis flange of the robot and the I-shaped connecting component of the polishing device. As a porous elastic material, although the primary function of the metal rubber is to provide damping to suppress vibrations (Figure 3), it inherently functions as a high-damping device that also possesses explicit stiffness characteristics. This type of vibration damper does not operate independently; its mechanical behavior is closely correlated with the equivalent stiffness of the robot's end-effector. Therefore, it is essential to analyze the coupling relationship between the two within a unified theoretical framework.

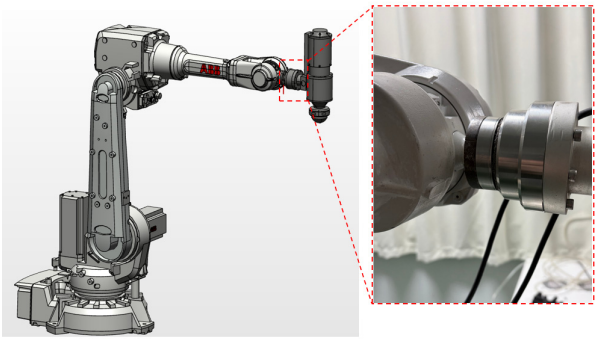

Figure 2. Vibration damping device of the airbag polishing tool

The total stiffness of the vibration damper is given by $k_d = 3\times10^4\, N\cdot mm$, and its angular stiffness is given by $k_m = 1.2\times10^6\, N\cdot mm/\text{rad}$, It can be observed that the stiffness of the end-effector is an order of magnitude smaller than that of the robot joints. Consequently, the contribution of the vibration damper's compliance to the total system compliance is significant and cannot be neglected. Treating the damper as a rigid body would result in an overestimation of the system's calculated stiffness, thereby compromising the reliability of the subsequent posture optimization results.

Since the vibration damper primarily undergoes compressive deformation along the feed normal direction of the polishing tool (i.e., the Z-axis of the tool coordinate system) to absorb vibration energy, the6×6compliance matrix of the metal rubber damper in the tool frame can be expressed as:

$$C_m = diag\begin{pmatrix} 0 & 0 & \dfrac{1}{k_m} & 0 & 0 & 0 \end{pmatrix} \tag{7}$$

Let its transformation matrix relative to the base frame be expressed as:

$$T_m^t = \begin{bmatrix} R_m & p_m \\ 0 & 1 \end{bmatrix} \tag{8}$$

where R_m represents the rotation matrix from frame {m} to the base frame, and p_m denotes the position vector.

The coordinate frame transformation follows the compliance mapping rule of rigid body transformations. The transformed compliance matrix of the vibration damper can be expressed as:

$$C_m^t = R_m \cdot C_c \cdot R_m^T \tag{9}$$

Finally, by linearly superimposing the compliance of the robot's end-effector and that of the vibration damper, the comprehensive compliance matrix of the robotic bonnet polishing system incorporating the metal rubber damper is obtained:

$$C_c^{'} = C_c + C_m^t \tag{10}$$

From this equation, the equivalent stiffness of the sixth axis can be calculated as: $k_6^{'} = 1.16\times10^6\, N\cdot mm/rad$

The modified joint stiffness of the robot is given by:

$$K_c^{'} = \left(k_1, k_2, k_3, k_4, k_5, k_6^{'}\right) = \left(2.36\times10^9, 8.41\times10^8, 5.82\times10^8, 7.22\times10^7, 3.76\times10^7, 1.16\times10^6\right) N\cdot mm/rad \tag{11}$$

This equation represents the comprehensive stiffness integrating both the structural stiffness of the robot and the vibration damper. Consequently, it effectively addresses the inaccuracy of the original model caused by neglecting the stiffness of the end-effector.

3. Robot Stiffness Performance Indices

First, the compliance ellipsoid of the robot's end-effector is derived based on the comprehensive stiffness model. Second, the robot's performance evaluation indices are established according to the actual polishing operating conditions. Finally, the validity of these evaluation indices is verified through simulations.

3.1. Robot Compliance Matrix and Compliance Ellipsoid

From Equation (5), it can be seen that the compliance matrix is a 6×6 six-dimensional matrix, which describes the relationship between the generalized six-dimensional force F acting on the robot's end-effector and the resulting generalized six-dimensional displacement ΔX :

$$\Delta X = C_c^{'} \cdot F \tag{12}$$

This expression can be simplified [9] as:

$$d = C_{fd} f \tag{13}$$

where f denotes the end-effector force vector; C_{fd} is the force-translational compliance matrix (measured in mm/N), which represents the translational displacement of the end-effector generated when subjected to the force f; and d is the translational displacement vector of the end-effector.

Expanding this yields:

$$\begin{bmatrix} d_x \\ d_y \\ d_z \end{bmatrix} = \begin{bmatrix} c_{11} & c_{12} & c_{13} \\ c_{21} & c_{22} & c_{23} \\ c_{31} & c_{32} & c_{33} \end{bmatrix} \begin{bmatrix} f_x \\ f_y \\ f_z \end{bmatrix} \tag{14}$$

Let $\|d\| = d^T d = 1$ (the unit force vector). By combining this with the above equation, we obtain:

$$f^T C_{fd}^T C_{fd} f = 1 \tag{15}$$

This formula defines an ellipsoid in three-dimensional space with respect to the force vector f, as shown in Figure 4(a). Termed the robotic Cartesian compliance ellipsoid, this geometric representation visualizes the anisotropy of compliance and serves to describe the robot's static stiffness characteristics. Its eigenvalues $\lambda_1, \lambda_2, \lambda_3$ (assuming $\lambda_1 > \lambda_2 > \lambda_3$) can be obtained by performing an eigenvalue decomposition on the matrix $C_{fd}^T C_{fd}$, with the corresponding three unit column vectors v_1, v_2, v_3 representing the principal directions of the ellipsoid.

The center of this ellipsoid is located at the center of the robot's sixth-axis flange, as illustrated in Figure 4(c). However, during the actual polishing process, the ellipsoid at the contact point between the robot's end-effector and the workpiece (defined here as frame {T}) provides a more accurate representation of the robot's stiffness characteristics, as shown in Figure 4(d). A rotation matrix ${}^{6}_{TCP}T$ [2] is introduced to describe the transformation between these two frames.

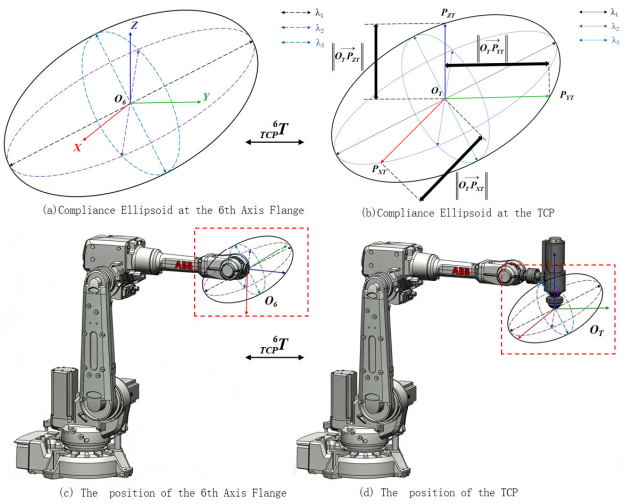

Figure 3. Schematic diagram of the robot Cartesian compliance ellipsoid

3.2. Robot Stiffness Performance Index

Combined with the force analysis during the bonnet polishing precession process (as shown in Figure 5), it is evident that the normal force in the Z-direction at the TCP plays a dominant role during dwell-point polishing. Consequently, the stiffness in this direction should be maximized to minimize robot deformation caused by process forces.Let P be the intersection point of the vectors along the X, Y, and Z axes with the surface of the compliance ellipsoid. As the robot's posture changes, the magnitudes and orientations of the ellipsoid's eigenvalues vary accordingly. However, the orientation of the X, Y, and Z axes within the machining plane remains relatively constant. This results in variations in the length of the line segment $O_T P_{ZT}$, as illustrated in Figure 4(b).Therefore, the essence of robot posture optimization for bonnet polishing is to manipulate the size and orientation of the compliance ellipsoid by adjusting the robot's configuration. The goal is to align the minor axis of the ellipsoid—representing the minimum eigenvalue, or the direction of minimum compliance and maximum stiffness—as closely as possible with the normal vector of the polishing contact point. This alignment ensures optimal stiffness, reducing chatter and deviation during the precession process and ultimately enhancing machining accuracy. Based on this physical insight, the robot stiffness evaluation indices are established.

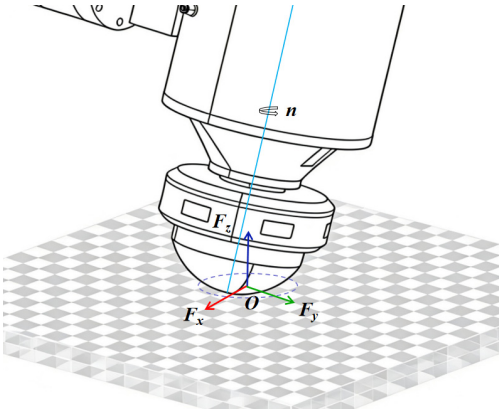

Figure 4. Analysis of Force Applied to Airbag Polishing

The compliance in the normal direction at the machining point is expressed as:

$$C_{ZT} = \left\| \overrightarrow{O_T P_{ZT}} \right\| \tag{16}$$

The corresponding stiffness is:

$$K_{ZT} = \frac{1}{C_{ZT}} = \frac{1}{\left\| \overrightarrow{O_T P_{ZT}} \right\|} \tag{17}$$

Based on the previous force analysis of the bonnet polishing process, the normal stiffness at the machining point should be maximized to resist robot deformation; therefore, the compliance at this point must be minimized. It is well-established that within an ellipsoid, the minimum value corresponds to the smallest eigenvalue λ_3. Since the orientation and magnitude of the compliance ellipsoid can be modulated by adjusting the robot's posture, the ultimate optimization objective is to align the direction of the ellipsoid's minor axis (representing the minimum compliance and maximum stiffness) as closely as possible with the normal direction. Accordingly, the normal stiffness evaluation index is defined as:

$$I_n = \frac{1}{\left\| \overrightarrow{O_T P_{ZT}} \right\|} \tag{18}$$

A larger value of I_n indicates a higher normal stiffness, implying that the robot is more capable of resisting deformation induced by process forces.

3.3. Finite Element Simulation Verification of the Robot Stiffness Performance Index

To verify the effectiveness of the comprehensive stiffness model and the normal stiffness evaluation index established in this paper, static structural simulation analyses were performed using ANSYS software to evaluate the robot's end-effector deformation resistance at typical polishing postures. Seven postures corresponding to different polishing points

were selected (as listed in Table 2). Two sets of simulation verifications—a control group and a verification group—were established: for the control group, the rotary joints of the robot model were assigned traditional joint stiffness values; for the verification group, the rotary joints were assigned the comprehensive equivalent stiffness values calculated in the previous sections $F = 47.52N$. A constant load was applied along the normal direction at the bonnet contact point, and the resulting end-effector deformations for both robot models were obtained (see Figure 6).

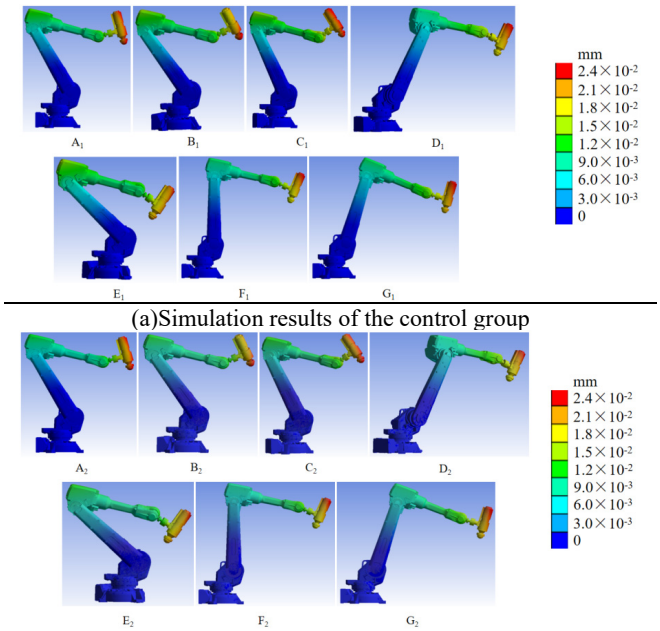

(a)Simulation results of the control group

(b)Simulation results of the verification group

Figure 5. Static simulation results

The deformation ΔX (mm×10^{-2})at the center of the air bag was extracted from the simulation, and the normal stiffness evaluation index I_n (N/mm)was calculated for the corresponding joint configurations. The results are summarized in Table 3. Given that the end-effector deformation under a constant load is inversely proportional to the robot's actual operational stiffness, the reciprocal of the deformation and the normal stiffness evaluation index were normalized to facilitate a quantitative comparison. The resulting two sets of curves are plotted in Figure 7.

As illustrated by the trends in Figure 7, the variations in the stiffness evaluation index are consistent with the simulated deformation patterns, which validates the correctness of the proposed index. Furthermore, the curve of the verification group shows a significantly higher degree of fit compared to the control group. This demonstrates that the comprehensive stiffness model can more accurately characterize the overall stiffness of the robotic polishing system after the integration of the metal rubber damper.

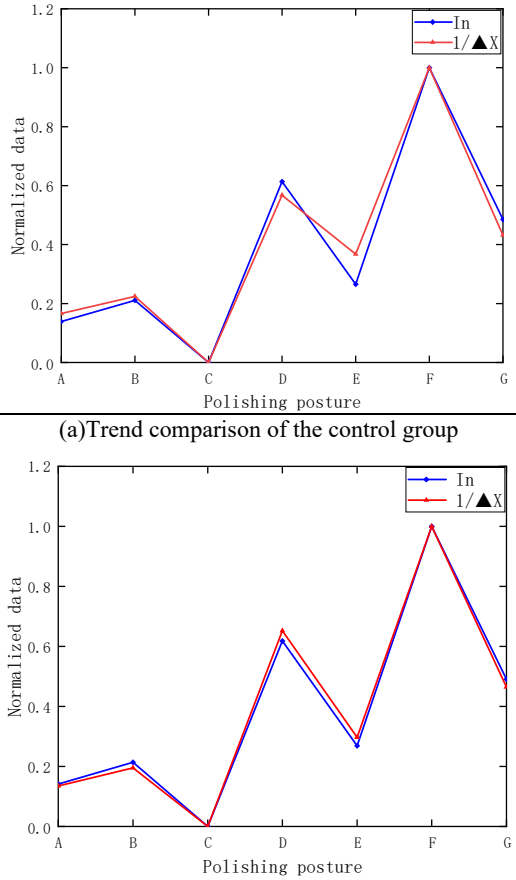

(a)Trend comparison of the control group

(b)Trend comparison of the verification group

Figure 6. Comparison of stiffness evaluation indicators and end deformation quantities

Table 2. Joint angles of the robots in seven different postures

Simulation Group Settings	J1(°)	J2(°)	J3(°)	J4(°)	J5(°)	J6(°)
A	0	-19	32	0	-31	0
B	20	-25	39	10	-43	15
C	-20	-20	27	0	-40	-15
D	0	27	-17	-10	10	0
E	30	-40	47	5	28	-20
F	0	18	0	0	-2	0
G	0	3	12	0	6	0

Table 3. Evaluation Indicators of Simulation Deformation and Stiffness

	Simulation Group Settings	A	B	C	D	E	F	G
control group	deformation ΔX	2.10	2.07	2.19	1.91	2.00	1.74	1.97
	normal stiffness evaluation index I_n	342.91	385.70	260.23	625.54	418.35	855.55	549.33
verification group	deformation ΔX	2.38	2.33	2.50	2.01	2.25	1.82	2.13
	normal stiffness evaluation index I_n	339.22	380.80	258.03	612.76	412.33	831.83	539.46

4. Robot Position Optimization Method and Verification

4.1. Optimization Objective Mathematical Mode

As shown in Figure 8(a), in the planar airbag polishing process, the normal force of the contact area can be equivalently concentrated at the center O of the airbag and perpendicular to the workpiece surface. To meet the requirements of the polishing process, the end posture of the airbag can be constrained and described by two key geometric parameters: the angle of rotation ρ between the airbag axis and the normal line of the polishing point (see Figure 8b); when ρ is constant, the continuous redundant airbag posture angles can be generated by the rotation α of the airbag axis around the plane normal line. To quantify this redundant angle, the airbag axis is projected onto the XOY plane and the positive direction of the Y-axis is taken as the zero position reference (see Figure 8c).

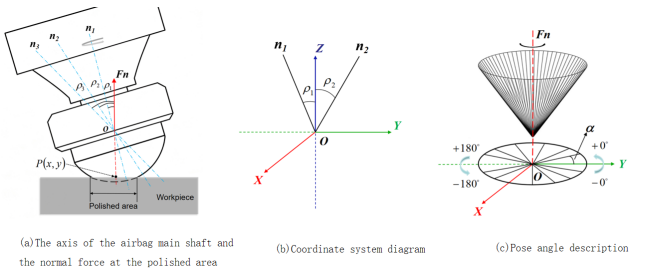

(a)The axis of the airbag main shaft and the normal force at the polished area (b)Coordinate system diagram (c)Pose angle description

Figure 7. The spatial relationship between the main axis of the airbag and the normal line of the plane

In the fixed-point polishing task, different combinations of precession angle xx and pose angle xx correspond to completely different robot joint configurations and end-effector stiffness distributions. Numerous studies have shown that the optimal precession angle range for airbag polishing is 15° to 25°. This paper sets the precession angle as a fixed 20° to study the optimal normal anti-deformation pose of the robot during polishing. An optimization mathematical model is established to investigate this condition. The optimization model includes constraints, objective function, and optimization variables: The constraints are the fixed polishing point in space and the robot joint motion space; the objective function is to maximize the normal stiffness evaluation index; the pose angle is the optimization variable. Finally, the optimized mathematical model obtained is:

$$\begin{cases} Find & \alpha \\ Max & I_n \\ s.t. & \begin{cases} P_0 \\ \theta_{i\min} < \theta_i < \theta_{i\max} \ (i = 1,2...6) \end{cases} \end{cases} \tag{19}$$

4.2. Optimization Algorithms and Results

This paper employs the Particle Swarm Optimization algorithm (PSO) [10]for optimization. It has the characteristics of few parameter settings and strong search capability.

For the fixed polishing point positions in the base coordinate system, the joint angles of the robot after optimization are obtained using Matlab. The obtained joint angles are: $q = [-2.51 \quad 18.95 \quad 20.96 \quad -12 \quad -17 \quad -0.31]$, Normal stiffness evaluation index $I_n = 1238.26(N/mm)$

4.3. Experimental Verification of the Optimization Results

By conducting fixed-point polishing of quartz glass under the same working conditions, the correctness of the pose optimization was verified. Four sets of different working poses that could reach the polishing points were selected, as shown in Figures 11(a, b, c, d). Except for the airbag pose angle and joint angles, all other relevant conditions were the same as the optimized pose. The corresponding normal stiffness evaluation indicators were calculated, where the number 5 represents the optimized pose. Key process parameters were set as follows: The airbag inflation pressure was set to 0.15 MPa constantly through the airbag main shaft control cabinet shown in Figure 10(a), the main shaft rotation speed was set to 802 r/min constantly, and the initial pressure on the workpiece was ensured to be ; the initial contact area between the airbag and the workpiece was ensured to be through the film pressure sensor shown in Figure 10(d), and the polishing liquid used was a fixed-concentration diamond polishing liquid. The surface roughness of the unpolished quartz glass was 0.101 μm, and the single-point polishing dwell time was 5 minutes.

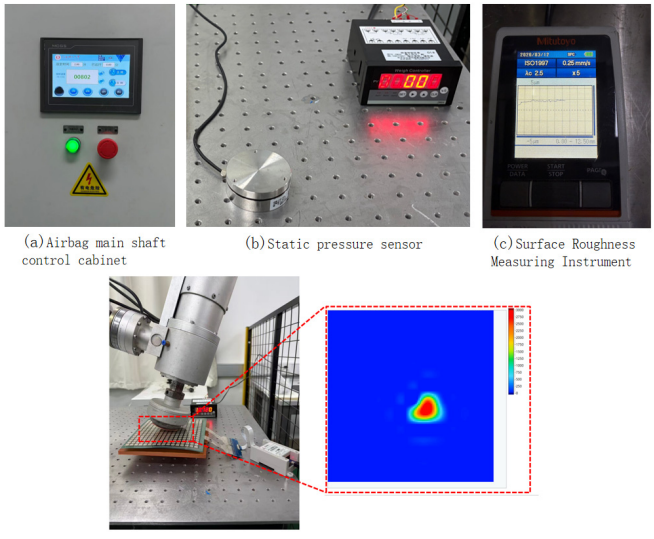

(a)Airbag main shaft control cabinet (b)Static pressure sensor (c)Surface Roughness Measuring Instrument

(d)Thin-film pressure sensor

Figure 8. Controller and Sensors

After polishing was completed, the polishing area morphology data of each group of samples were extracted using a surface roughness instrument, as shown in Figure 10(c), and the surface roughness data of 5 pieces of glass were obtained. To visually reveal the mapping relationship between the system stiffness and processing quality, the reciprocal of the surface roughness and the normal stiffness evaluation indicator were normalized, as shown in Figure 12. The results show that the surface roughness of the workpiece decreases significantly with the increase of the normal stiffness of the robot end; the optimal pose obtained by the algorithm has the best normal stiffness performance and the lowest surface roughness, confirming the correctness of the pose

optimization.

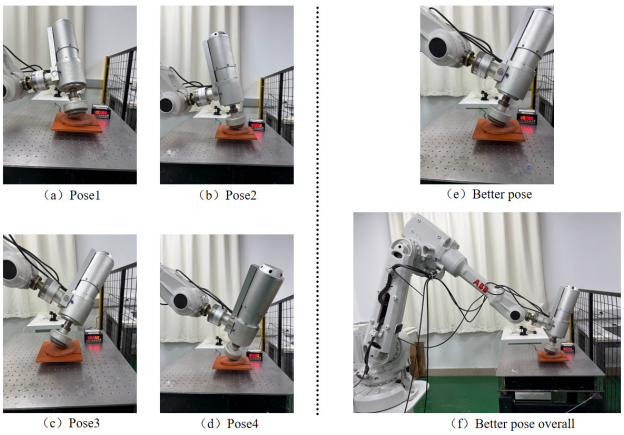

Figure 9. Comparison of the original pose and the optimized pose

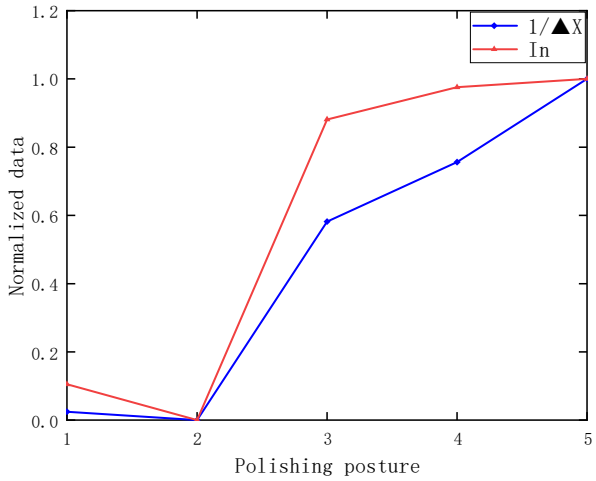

Figure 10. Relationship between normal stiffness evaluation index and surface roughness

Table 4. Evaluation Indicators of Corresponding Normal Stiffness Based on Different Airbag Positioning Angles

Control group number	Airbag position angle α (°)	Joint angleq	I_n (N/mm)	Surface roughness after polishing (μm)	
1	15	$q_1 = [3.75 \quad 19.58 \quad 29.84 \quad 0 \quad -48 \quad -25]$	268.11	0.075	
2	90	$q_2 = [-1.07 \quad 19.58 \quad 35.16 \quad 0 \quad -68 \quad 0]$	148.72	0.079	
3	-30	$q_3 = [0 \quad 20.89 \quad 16.56 \quad -13 \quad -7.5 \quad -8.33]$	1126.50	0.035	
4	-120	$q_4 = [-3.75 \quad 21.3 \quad 16.56 \quad -13 \quad -10 \quad 29.17]$	1217.38	0.030	
5	-53.8	$q_5 = [-2.51 \quad 18.95 \quad 20.96 \quad -12 \quad -17 \quad -0.31]$	1238.26	0.025	

5. Conclusion

This paper addresses the issue of weak structural stiffness in the ABB IRB2600 robotic bonnet polishing system after incorporating a metal-rubber damping device. The research focuses on the comprehensive stiffness modeling of the system and pose optimization, aiming to enhance polishing stability and surface quality. The main research work and conclusions are as follows:

(1) A kinematic model of the robot was established using the modified D-H parameter method, and the Jacobian matrix was derived. Based on the classical joint stiffness model, the equivalent angular stiffness of the metal-rubber damping device was introduced. A comprehensive system stiffness model was constructed using the flexibility superposition principle, correcting the error of traditional models that neglect the flexibility of the end-effector. Finite element simulations verified that the model's calculation results align with the trend of end deformation.

(2) Combining the flexibility ellipsoid theory with the force characteristics of polishing, a normal stiffness evaluation index was proposed to achieve quantitative assessment of the robot's stiffness performance. This index shows a significant negative correlation with end deformation, providing a quantitative basis for pose optimization.

(3) The concept of the bonnet pose optimization angle was introduced. Using this angle as the optimization variable and maximizing normal stiffness as the objective, an optimization model was established with constraints including joint limits and precession angle. The PSO algorithm was employed to solve the model, yielding an optimal pose angle of -53.8°, corresponding to a normal stiffness of 1238.26 N/mm.

(4) Polishing experiments on quartz glass demonstrated that the surface roughness of the workpiece was reduced from 0.1μm to 0.025μm after adopting the optimized pose, showing significant improvement in surface quality compared to other poses. This validates the engineering effectiveness of the proposed model and optimization method, indicating that enhancing normal stiffness effectively suppresses end deformation and improves processing quality.

References

[1] Lin Zewen. Research on robot airbag polishing technology and process for optical elements[D]. Master's Thesis of Xiamen University, 2020.

[2] Ri Pan, Wanying Zhao, Zhenzhong Wang, Shuting Ji, Xiangsheng Gao, Dongju Chen, Jinwei Fan, Research on an evaluation model for the working stiffness of a robot-assisted bonnet polishing system,Journal of Manufacturing Processes, Volume 65,2021,Pages 134-143,ISSN 1526-6125,https:// doi. org/ 10.1016/j.jmapro.2021.03.013.

[3] Qu Weiwei, Hou Penghui, Yang Genjun, et al. Research on Stiffness Performance Optimization of Robotic Machining System[J]. Acta Aeronautica et Astronautica Sinica, 2013, 34 (12): 2823-2832.

[4] Z hu Tianyu, Hong Rongjing, Zhang Hao, et al. Pose Optimization of Robot Chamfering Based on Stiffness and Kinematic Performance[J]. Combined Machine Tool &

Automatic Manufacturing Technique, 2025, (09): 55-60. DOI: 10.13462/j.cnki.mmtamt.2025.09.011.

[5] Zhou Yongyu, Jiang Chen, Jiang Zhenyu, et al. Dynamic Characteristic Analysis and Optimization Research of Airbag Polishing Robot[J]. Machinery & Electronics, 2024, 42(10): 61-68.

[6] Wang Lili. Research on Motion Planning and Vibration Suppression of Forging Robot[D]. Jiangsu University of Science and Technology, 2021. DOI: 10.27171/d.cnki. ghdcc. 2021. 000080.

[7] Yin Haibin. Rigid-Flexible Coupling Dynamics—Mechanical Basis for Design and Control of Lightweight Collaborative Robots--Interpretation of *Rigid-Flexible Coupling Dynamics of Robots*[J]. China Mechanical Engineering, 2018, 29(24): 3020-3023.

[8] DENAVIT J, HARTENBERG R S. A kinematic notation for lower-pair mechanisms based on matrices[J]. Journal of Applied Mechanics, 1955, 22(2) : 215-221.

[9] SALISBURYJK.Active stiffness control of a manipulatorin cartesian coordinates[J].Decision and Control Includingthe Symposium on Adaptive Processes, 1980 19th IEEE Conference on, 1980, 19: 95−100.

[10] Fang Jun. Research on Particle Swarm Optimization Algorithm and Its Application[D]. Chengdu: University of Electronic Science and Technology of China, 2006.